# Study of a pseudo-empirical model approach to characterize plasma actuators



2011 J. Phys.: Conf. Ser. 296 012023

(http://iopscience.iop.org/1742-6596/296/1/012023)

FLUIDOS 2010: XI Meeting on Recent Advances in the Physics of Fluids and their Applications IOP Publishing
Journal of Physics: Conference Series **296** (2011) 012023 doi:10.1088/1742-6596/296/1/012023

# Study of a pseudo-empirical model approach to characterize plasma actuators

**M Marziali Bermudez[1], R Sosa[2,4], D Grondona[3], A Márquez[3], H Kelly[3] and G Artana[2,4]**

[1]Departamento de Física, Facultad de Ciencias Exactas y Naturales, UBA, Ciudad Universitaria Pab. I, Buenos Aires 1428, Argentina
[2]Laboratorio de Fluidodinámica, Facultad de Ingeniería, UBA, Av. Paseo Colón 850, Buenos Aires 1063, Argentina
[3]Instituto de Física del Plasma (CONICET) - Departamento de Física, Facultad de Ciencias Exactas y Naturales, UBA, Ciudad Universitaria Pab. I, Buenos Aires 1428, Argentina
[4]CONICET

E-mail: rsosa@fi.uba.ar

**Abstract.** The use of plasma actuators is a recent technology that imposes a localized electric force that is used to control air flows. A suitable representation of actuation enables to undertake plasma actuators optimization, to design flow-control strategies, or to analyse the flow stabilization that can be attained by plasma forcing. The problem description may be clearly separated in two regions. An outer region, where the fluid is electrically neutral, in which the flow is described by the Navier-Stokes equation without any forcing term. An inner region, that forms a thin boundary layer, where the fluid is ionized and electric forces are predominant. The outer limit of the inner solution becomes the boundary condition for the outer problem. The outer problem can then be solved with a slip velocity that is issued from the inner solution. Although the solution for the inner problem is quite complex it can be contoured proposing pseudo-empirical models where the slip velocity of the outer problem is determined indirectly from experiments. This pseudo-empirical model approach has been recently tested in different cylinder flows and revealed quite adapted to describe actuated flow behaviour. In this work we determine experimentally the influence of the duty cycle on the slip velocity distribution. The velocity was measured by means of a pitot tube and flow visualizations of the starting vortex (i.e. the induced flow when actuation is activated in a quiescent air) have been done by means of the Schlieren technique. We also performed numerical experiments to simulate the outer region problem when actuation is activated in a quiescent air using a slip velocity distribution as a boundary condition. The experimental and numerical results are in good agreement showing the potential of this pseudo-empirical model approach to characterize the plasma actuation.

## 1. Introduction

Electro-hydrodynamic (EHD) actuators for flow control with aims to improve aerodynamic design have been receiving special attention in the last years [1, 2, 3]. Through the ionization of the flowing air close to the surface of a body, EHD devices produce a modification of the condition of the flow at the wall proximity. The charged particles present in the ionized air (plasma) experience an electric force that is transmitted through particle collision to the neutrals of the flowing air. The expression of this force on the fluid depends on the discharge characteristics, and in some cases there exists a two-way interaction created by electric forces as they elicit a

mechanical response that, in turn, alters the fields. The implementation of this force in numerical flow simulations is of interest, as it could be used to optimize the design and placement of plasma actuators for different applications for flow control.

Detailed studies on how to implement the electric force coupling in validated codes of computational fluid mechanics as direct numerical simulations (DNS) have been reported for the relatively simple cases of classic corona discharges [4]. For the specific case of dielectric barrier device (DBD) actuators, which we study here, efforts have been also reported recently by different researchers [1, 2, 5].

A recent computational exploration has been conducted by Visbal et al. (2006) [6] using large-eddy simulation approaches at a Reynolds number $Re \approx 10^4$ in order to capture the effects of the local forces of the DBD device on turbulent, separated flows. Unfortunately, these researches also concluded that further work was still needed in order to construct detailed models for the spatio-temporal distribution of the plasma-induced body forces suitable for incorporation into flow simulations.

Corke et al. [5] derived a simplified expression for the body force distribution and implemented it in the numerical flow solver CFL3D [7] to estimate the aerodynamic coefficients involved in the control of leading-edge separation on wing sections. Likhanskii et al. [8] developed a more detailed physical model for DBD in air, and noted the computational difficulties of plasma numerical simulation over large temporal and spatial scales. They concluded that in general, the cell size for the rectangular grid has to be chosen according to the characteristics of plasma and voltage scales and geometrical size (on the order of 10 microns); this in turns requires an extremely high number of computational points in order to perform calculations in large scale geometries (i.e., beyond the domain which is next to the electrode configuration) or multielectrode arrangements.

The other difficulty in plasma-effects simulations is the choice of the time step. Because the time step should allow for the resolution of plasma formation and streamer propagation dynamic time (which is of the order of nanoseconds), this time scale must be several orders of magnitude smaller than the time scale over which the plasma is producing an effect on the surrounding air. Therefore, both factors make prohibitive an easy approach to detailed plasma actuation over large spatio-temporal scale using DNS.

The use of some approximated models (empirical or quasi-empirical) to evaluate the plasma actuation are in consequence attractive. The possibility to attain realistic models is however better when flow characteristic frequencies result much lower than those of cyclic excitation of the discharge (usually some kHz). Flows can then be considered steadily excited with a time averaged plasma forcing that is determined under controlled experimental conditions and then extrapolated to the case of interest.

On the other hand, the region where the momentum transfer from ions to neutrals can occur is confined to a very narrow region quite similar to streamer radius. This region is extremely thin compared to most fluid dynamics characteristic lengths of reference.

Under these circumstances the full problem description may be clearly separated in two: an outer and an inner problem. At the outer region we have fluid that is electrically neutral and is described by the Navier-Stokes equation without any forcing term. In the inner region at the discharge region we have a thin boundary layer where the electric forces are confined.

Opaits et al. [9] have proposed a new approach for non-intrusive diagnostics of plasma actuator induced flow in quiescent gas. This approach consisted in using the force calculated by the plasma model [7] as an input to a two-dimensional viscous flow solver to predict the time-dependent DBD induced flow and then to match this numerical result with Schlieren images of the induced flow. Thus this approach allowed to restore the entire two-dimensional unsteady plasma induced flow pattern as well as characteristics of the plasma induced force.

In the present work we propose to solve the outer problem imposing a slip velocity as

a boundary condition. A similar approach has been used in other problems with similar characteristics like for instance in electrosmotic flows [10]. The solution for the inner problem is quite complex in general but can be contoured proposing pseudo-empirical models where the slip velocity of the outer problem is determined indirectly from experiments. A large number of efforts have been done by different authors that have measured for different kind of plasma actuators the velocity profiles induced by the discharge with different techniques like laser doppler velocimetry or pitot tubes. It can be observed that actuation produces in most cases a pulsed type distribution, with its width and peak value depending on electrical parameters of the actuator excitation signal (amplitude, frequency, shape type) and constructive characteristics (spacing, dielectric thickness, dielectric material).

This pseudo-empirical model approach has been also recently tested in different cylinder flows and revealed quite adapted to describe actuated flow behavior [11, 12, 13].

The goal of this article is to determine how the actuation representation has to be adapted when considering different actuation intensities.

## 2. Experimental set-up

### *2.1. Electrodes arrangement and electric circuit*

Figure 1 shows a scheme of the electrode arrangement and the electric circuit. The electrode arrangement consists of an air-exposed electrode flush mounted on a Kapton® foil (electrode (1), width 20 mm) and an electrode located on the opposite side (electrode (2), width 5 mm). Both electrodes are made of aluminum foils and they are about 50 $\mu$m thick. The Kapton® foil, with the electrodes, was stuck on the surface of a 4mm thick PMMA flat plate.

The electrode exposed to the air (electrode (1)) was connected to the output of an AC power supply (peak-to-peak voltage $V_{AC}$ in the range 0–23 kV) and the encapsulated electrode (electrode (2)) was grounded. Thus the plasma actuator induces a mean flow as sketched on figure 1.

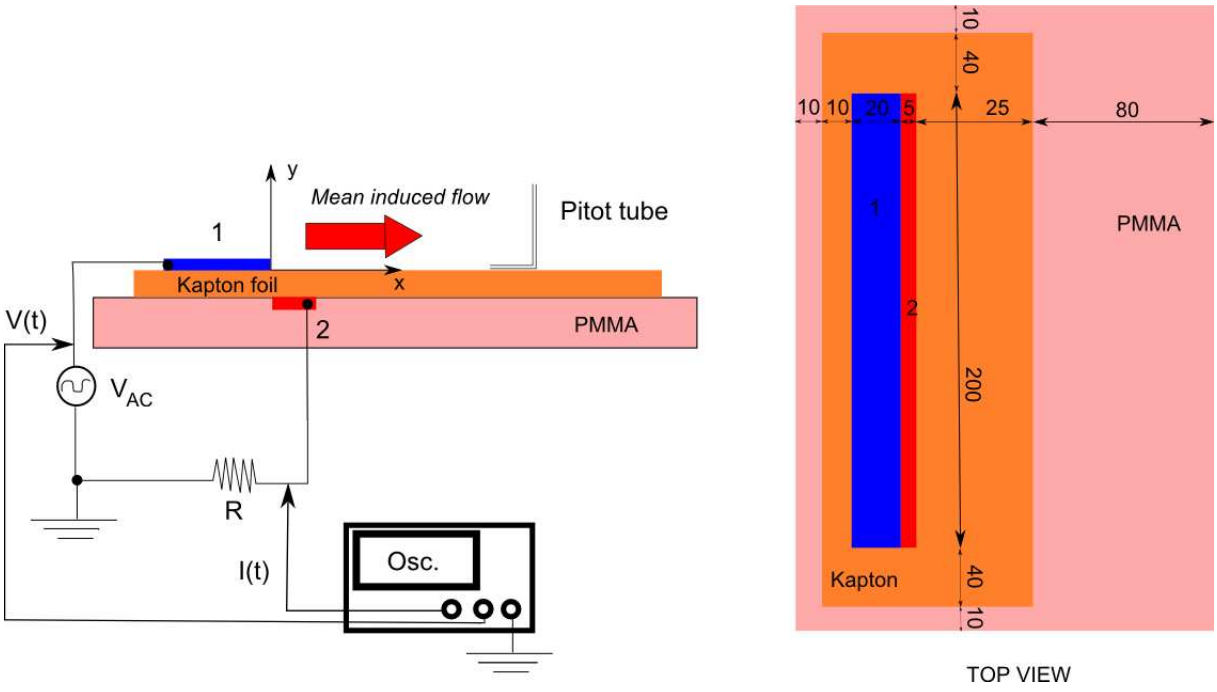


**Figure 1.** Electrodes arrangement and electric circuit (dimensions are in mm)

The AC power supply consisted of a function generator coupled to an audio-amplifier (of 700 W) that fed a high voltage transformer coil. In practice there was an optimal matching frequency, established by the resonance between the transformer inductance and the stray capacity of the electrode arrangement, including the wire connections. For our circuit geometry, the optimum excitation AC frequency was $f_{AC} = 5.5$ kHz ($T_{AC} = 1/f_{AC} = 180$ $\mu$s).

The DBD current ($I(t)$) measurement was performed by connecting electrode (2) through a 50 $\Omega$ resistance to the ground and registering the voltage drop on this resistance. The instantaneous voltage applied to electrode (1), $V(t)$, was measured with a HV probe (1000X, 3.0 pF, 100 M$\Omega$). These electrical signals were registered by using a four-channel digitizing oscilloscope with an analog bandwidth of 60 MHz and 1 GS/s sampling rate.

The signal generator can operate the DBD by burst modulation of the sinusoidal high voltage signal. The effect of the duty-cycle (defined as: $100 \times T_{ON}/T_{BM}$, being $T_{ON}$ the time during which the plasma is produced, see figure 2) was explored for values from 35% up to 100%. This parameter quantifies the fraction of time that the discharge, and consequently the forcing, is active. Thus by changing this parameter it is possible to modify the time averaged intensity of actuation.

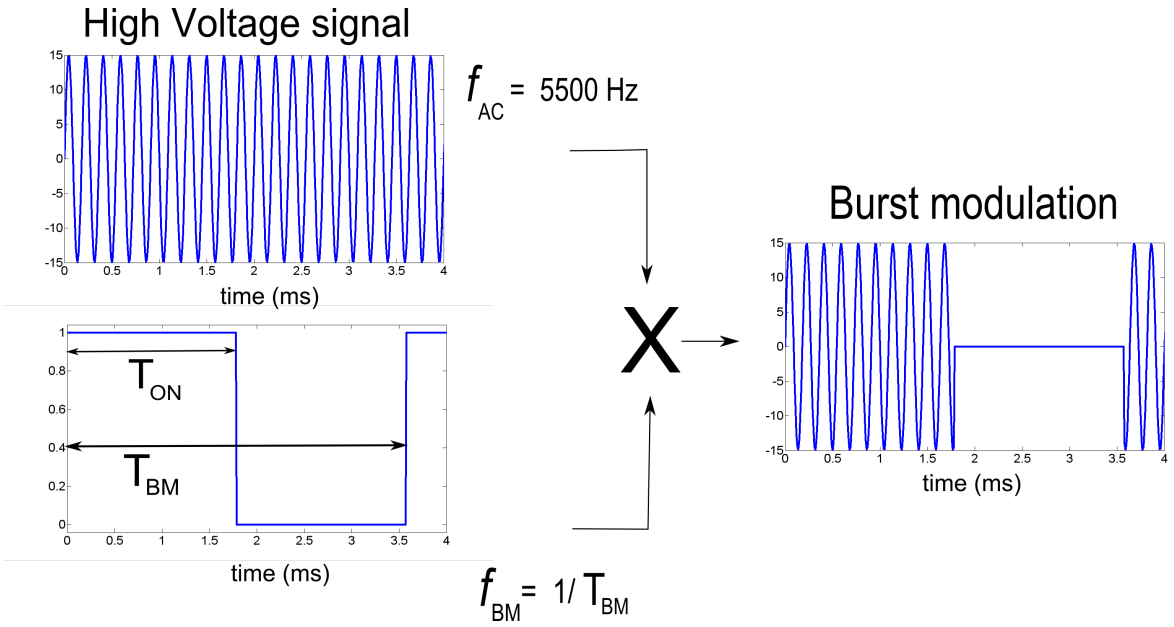


**Figure 2.** Burst modulation mode ($f_{BM} = 280$ Hz, duty-cycle 50% as an example)

In our studies $T_{BM}$ was fixed to a value of $T_{BM} = 20 \times T_{AC} = 3.6$ ms in order to assure at least seven cycles of the high voltage signal for the lower duty-cycle considered. This choice guarantees that the distribution of charges on the surface settles into an equilibrium configuration [14].

*2.2. Schlieren visualization setup*

To visualize the induced ionic wind a Schlieren system disposed in a Z configuration was used [15]. It comprised two spherical mirrors of 50 cm in diameter and 3.0 m in focal length. The light (a tungsten-halogen automotive lamp) was cut off with two razor blades at the meridional and sagittal focal planes. Thus 2D density gradients could be detected. The images were recorded on a monochromatic digital image camera of 12 bits that enabled fast frame acquisition (up to 200 fps). The Schlieren technique is able to detect changes in index refraction associated to density gradients in a fluid media. In general the small changes in density associated to

the heating produced by the discharge enable to obtain images with sufficient contrast. In this context the tracers are the same fluid particles (the studied ones) and therefore there is not need to introduce any external particles (like smoke particles in the PIV systems).

*2.3. Pitot tube measurement setup*

Velocity measurements are conducted with the help of a Pitot tube. This was made of electrically insulating glass tube (internal diameter: ID = 0.70 mm, outer diameter OD = 0.97 mm) and was connected by mean of a tygon tube to a differential pressure transducer of variable reluctance type (0 to 55 Pa, accuracy of 0.25% full scale). The reference pressure value was measured far away from the electrodes. This pressure sensor may be displaced along the $x$ and $y$ axes (see figure 1), and the goal is to plot velocity the profiles above the wall (with the pitot on the wall, that is $y = 0.49$ mm) at different $x$ positions.

## 3. Numerical simulation

*3.1. General characteristics of the simulation code*

The geometry has been non-dimensionalized with the electrode (2) width. The computational geometry is defined by a rectangle placed with dimensions $L = 12$ and $H = 4$. The center of coordinates is placed at the bottom surface of the box and 4 units ahead of the left vertical surface (see figure 3).

The boundary conditions can be divided in three sections: $\Gamma_P$ composed of the Kapton® surface above the electrode (2) and associated to the plasma region, $\Gamma_W$ composed of the rest of the solid surfaces (Kapton® and PMMA) where no plasma is produced and no slip is considered. Finally for the rest of the surfaces, $\Gamma_N$, where natural boundary conditions (NBC) have been used (see equation 4). For the Kapton® surface, above the electrode (2), $\Gamma_P$ the boundary condition comes from the slip velocity imposed by the plasma actuator and is given by the equation

$$v_i(x) = \frac{A}{W\,x} \mathrm{e}^{-\frac{1}{2}\left(\frac{\log(x-x_0)}{W}\right)^2} \hat{\mathbf{e}}_x \tag{1}$$

where the log-normal function $v_i(x)$ has three parameters: $A$, $W$ and $x_0$. $W$ is related to the pulse width, $A$ is related to the pulse amplitude and $x_0$ is related to the position of the maximum velocity. In the present study $W$ and $x_0$ were fixed and only the influence of the pulse amplitude was explored (see figure 3).

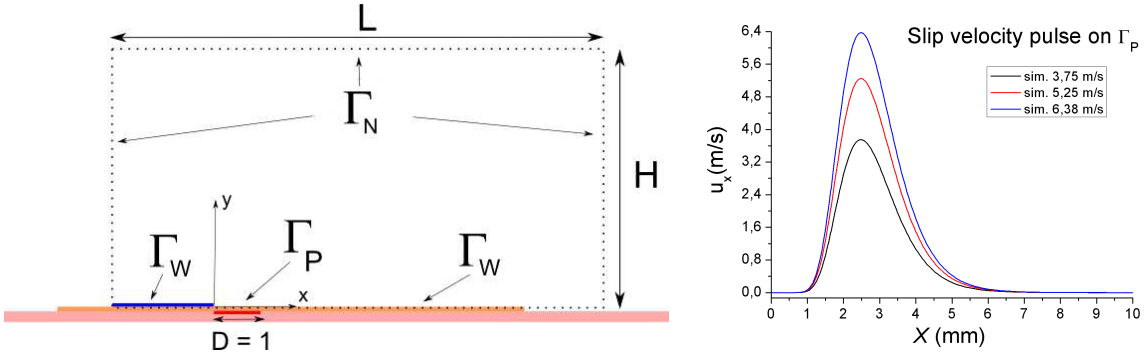


**Figure 3.** Scheme of the numerical domain and boundary conditions (left) and typical slip velocity pulse used as a boundary condition on $\Gamma_P$ (right).

*3.2. Governing equations*

Mass and momentum conservation principles are represented by the Navier-Stokes equations, which have the following form for an incompressible fluid:

$$\frac{\partial u_i}{\partial x_i} = 0 \quad \text{in } \Omega \tag{2}$$

$$\frac{\partial u_i}{\partial t} + u_j \frac{\partial u_i}{\partial x_j} = -\frac{\partial p}{\partial x_i} + \frac{1}{Re}\frac{\partial^2 u_i}{\partial x_j^2} \quad \text{in } \Omega \tag{3}$$

The boundary conditions were:

$$0 = -p\, n_i + \frac{1}{Re}\frac{\partial u_i}{\partial n} \quad \text{on } \Gamma_N \tag{4}$$

$$u_i = v_i \quad \text{on } \Gamma_P \tag{5}$$

$$u_i = 0 \quad \text{on } \Gamma_W \tag{6}$$

Here, $\Omega$ is the computational domain, $p$ the pressure divided by the (constant) mass density, $u_i$ is the $i^{\text{th}}$ component of the velocity field and $n$ is the outward unit-normal to the boundary.

To solve this equation we used a previously tested DNS code whose references can be found at [16].

## 4. Experimental and numerical results

*4.1. Schlieren visualization and vortex core trajectory*

The left-hand side of figure 4 shows a typical starting vortex for a high level of actuation. Because Schlieren imaging records variations in optical density, the hot air surrounding the electrode acted as a tracer. The tracer is then advected by the stream and diffuses mainly because of thermal effects. To improve these images, two laminar circular jets of helium have been added in these tests to obtain information where the thermal tracers are not present. In the right-hand side of figure 4 we show the isolines of the modulus of velocity obtained from our numerical simulations. The momentum injected in the discharge region is transported by the fluid and diffusion occurs as a consequence of viscosity. The evident physical correspondence in both cases is notorious.

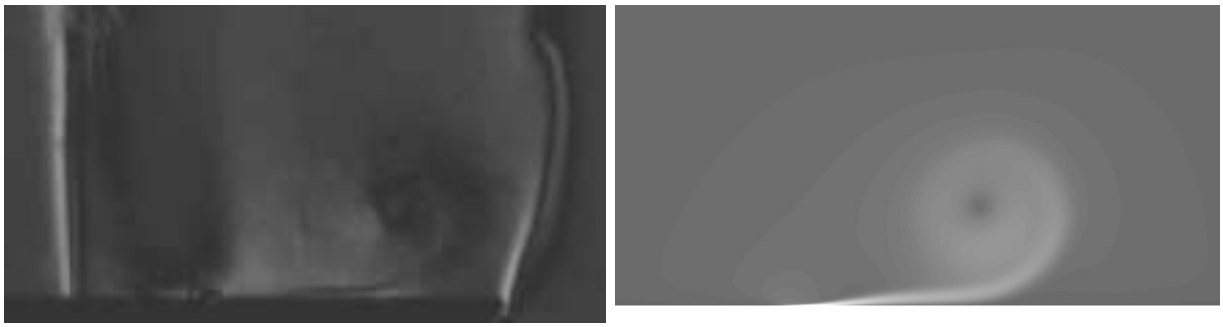

**Figure 4.** Results for high levels of actuation intensity: experimental imaging (left) and isolines of velocity modulus from simulation (right)

Figure 5 shows typical Schlieren images for reduced levels of actuation (no helium jets were incorporated in these experiments). The images show the starting vortex for $V_{AC} = 7$ kV, with 80% duty cycle. In order to track the starting vortex the image sequences obtained by the Schlieren technique were analyzed using the software *ImageJ*.

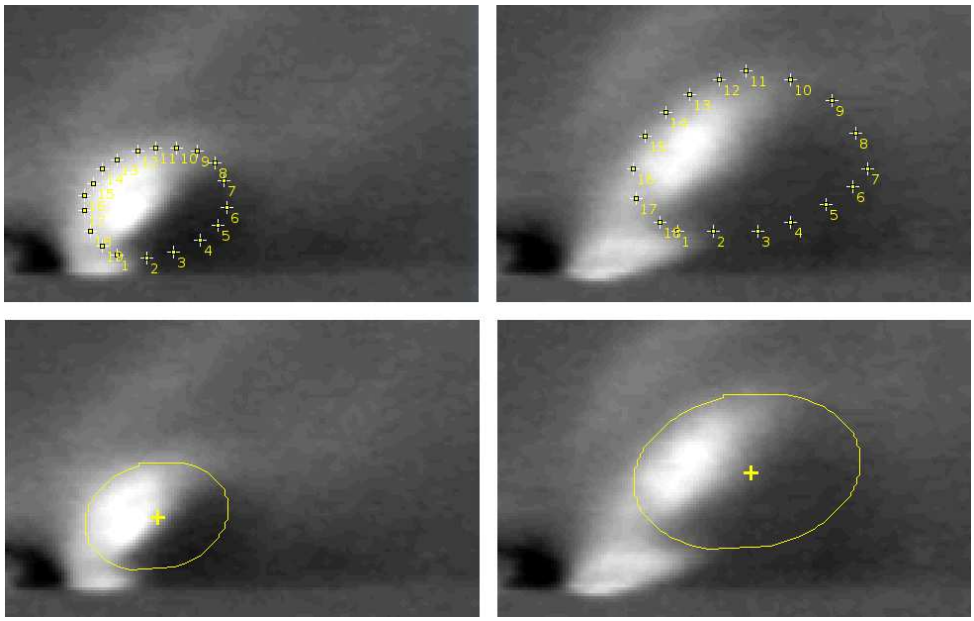

**Figure 5.** Schlieren images of the starting vortex for $V_{AC} = 7$ kV and 80% duty cycle. Time between images 10 ms, image size 10.5 mm x 6.5 mm.

Due to the low level of actuation intensity and due to thermal diffusion, the vortex center could be hardly determined directly. Therefore, a set of several points were laid around the vortex contour, as shown in the figure 5 (top), and an ellipse was fitted to those points (bottom). The centroid of such ellipse was considered to behave similarly enough to the actual vortex center within the scope of this study.

Figure 6 shows the $x$ position of the centre of the vortex as a function of time ($x_C$ vs. $t$, left figure) and the trajectory of the centre of the vortex ($x_C(t)$ vs. $y_C(t)$, right figure) for different duty-cycles and with $V_{AC} = 7$ kV.

As it can be observed, the vortex velocity (i.e. the slope of the curves $x_C$ vs. $t$) increase with the duty-cycle. On the other hand, the starting vortex seems to have almost the same trajectories, within our experimental uncertainty, independently of the duty cycle considered.

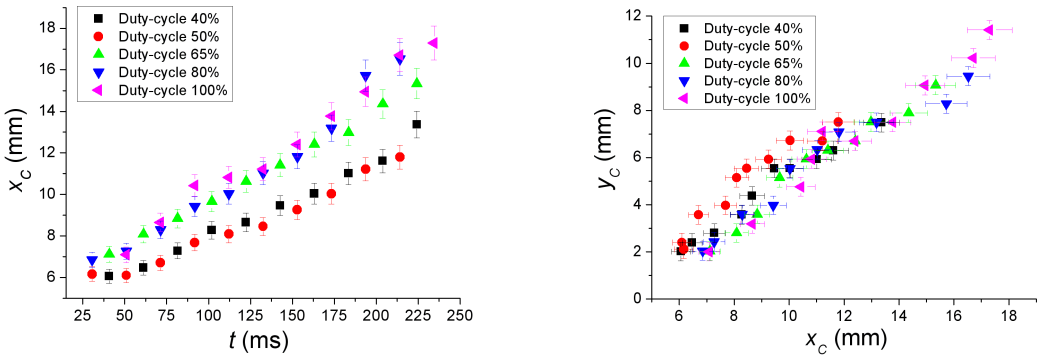


**Figure 6.** Left: $x_C$ vs. $t$. Right: trajectory of the centre of the vortex, $x_C(t)$ vs. $y_C(t)$. For different duty-cycles and with $V_{AC} = 7$ kV.

*4.2. Comparison between experimental and numerical results*

*4.2.1. Starting vortex trajectory* Figure 7 shows a typical velocity field obtained from numerical simulation. When the absolute value of the velocity is plotted, a clear unsteady vortical structure is observed and it is quite simple to determine their centre as it is shown in figure 7. Following this procedure we can reconstruct the $x$ position of the vortex center as a function of time and the trajectory of the centre of the vortex (for different amplitudes of the imposed slip velocity pulse) in order to compare that with the experimental results previously showed.

Figure 8 compares the curves of $x_C$ vs. $t$ (left) and $x_C(t)$ vs. $y_C(t)$ (right) obtained from experimental and numerical results. In the case of the experimental results we have plotted the cases of 40%, 65% and 100% of duty cycle only to simplify the graphics. On the other hand, the numerical results correspond to the cases of: 3.75 m/s, 5.25 m/s, 6.38 and 7.50 m/s of pulse amplitude.

We see that the numerical results agree quite well with the experimental ones, showing that the vortex central velocity and trajectories display the same dependence with respect to the duty-cycle value.

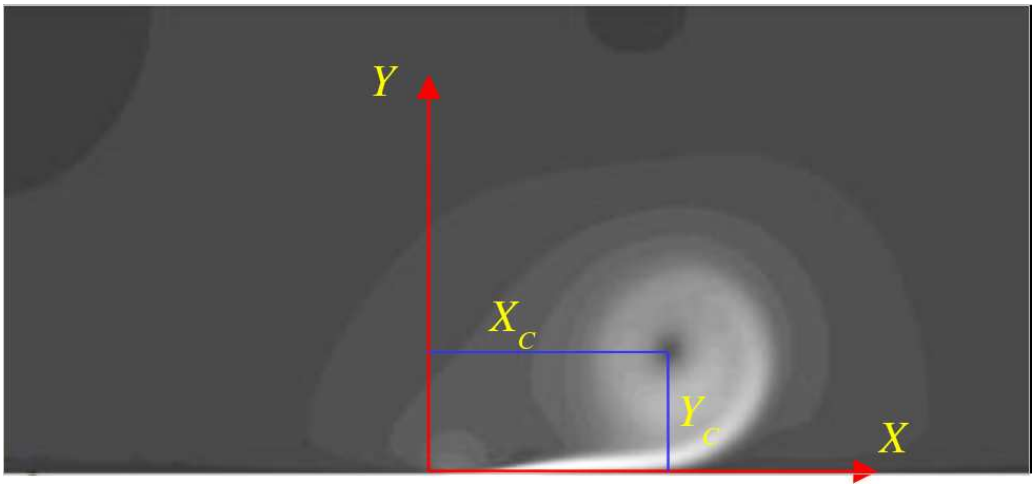


**Figure 7.** Typical velocity field obtained from numerical simulation.

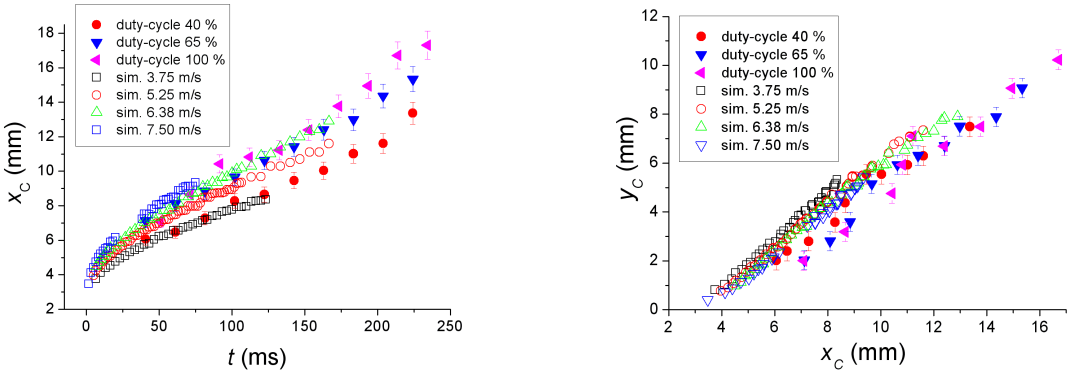


**Figure 8.** Plots of $x_C$ vs. $t$ (left) and $x_C(t)$ vs. $y_C(t)$ (right) obtained from experimental and numerical results. Experimental results for $V_{AC} = 7$ kV and duty-cycles of: 40%, 65% and 100%. Numerical results for pulse amplitudes of: 3.75 m/s, 5.25 m/s, 6.38 and 7.50 m/s.

It is important to note that the starting vortex behaviour described previously can be explained if we consider the similarity between this vortex structure and the junction vortex.

When an impulsively started moving wall slides under a stationary wall, the potential exists for a vortical structure to develop close to their junction. The formation mechanism for this vortex when the wall is set in motion, is that a Stokes layer develops over the moving surface and this layer is driven, by shear forces, past the singularity at the junction and over the stationary wall. Vorticity of opposite sign then develops over the stationary wall to enforce the no-slip condition. The flow field over the stationary wall initially resembles an unsteady wall jet. During an experiment, the circulation swept into the junction region can be defined as $\Gamma(t) = \int_0^t U_W^2(\tau)\mathrm{d}\tau$, where $U_W$ is the wall speed. This results in a Reynolds number, or non-dimensional time, defined as: $Re_\Gamma(t) = \frac{\Gamma(t)}{\nu}$, being $\nu$ the kinematic viscosity. If the Reynolds number is large enough, then the jet separates and rolls into a vortex [17].

Allen and Naitoh [17] have demonstrated that the unsteady junction vortex flow field is universal for a given $Re_\Gamma$ when the dimensions of the structure are non-dimensionalized with $\frac{U_W}{\nu}$ and the velocity is non-dimensionalized with $U_W$. Thus the vortex core coordinates ($x_C$, $y_C$) can be fitted with power law such as $\frac{x_C\,U_W}{\nu} = \kappa_x(Re_\Gamma)^{q_x}$ and $\frac{y_C\,U_W}{\nu} = \kappa_y(Re_\Gamma)^{q_y}$.

In our study $U_W$ can be assumed constant (because the $V_{AC}$ value was fixed in all the experiments) resulting the Reynolds number equal to: $Re_\Gamma(t) = \frac{\Gamma(t)}{\nu} = \frac{U_X^2 t}{\nu}\frac{T_{ON}}{T_{BM}}$. Thus, $x_C$ and $y_C$ are time and duty-cycle (i.e. $T_{ON}/T_{BM}$) dependent. This last conclusion allows to explain the observed dependence of the vortex core velocity on the duty-cycle.

On the other hand, it is easy to demonstrate mathematically that the vortex core trajectory (i.e. $y_C$ as a function of $x_C$) does not depend on the duty-cycle. This can explain the fact that the experimentally observed curves $y_C(x_C)$ are almost coincident.

*4.2.2. Velocity profiles* In order to have another tool that allow us to validate our numerical simulations we have measured the horizontal component of the velocity ($u_x$) with the pitot tube resting on the surface (thus the central line of the pitot was at $y = 0.49$ mm).

For the values of pulse amplitude that recover quite well the vortex dynamics, in the numerical experiments, we have searched the value of $y$ that best fit our pitot measures.

Figure 9 shows the measured velocity profiles considering different duty cycles and the velocity profiles from numerical simulations (for $y = 0.15$, and considering different pulse amplitudes).

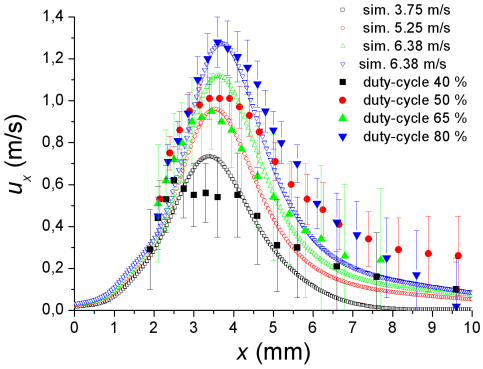


**Figure 9.** Velocity profiles from Pitot measurements ($y = 0.49$ mm, and duty cycles of: 40%, 50%, 65% and 80%. $V_{AC} = 7$ kV ) and numerical simulations ($y = 0.15$, and considering pulse amplitudes of: 3.75 m/s, 5.25 m/s, 6.38 and 7.50 m/s.)

The measured velocity profiles behave quite similar to the numerical ones. The observed discrepancies in terms of the $y$ coordinate can be explained considering that both the wall proximity and the intense velocity gradient close to the wall tend to produce a higher velocity measurement with the pitot tube. On the other hand, in the slip velocity model, the thickness of the inner region is neglected. If we assign to this region a thickness of 0.35 mm experimental and numerical results then are in a very good agreement.

## 5. Conclusions

In this work we have determined experimentally the influence of the duty cycle on the slip velocity distribution necessary to reproduce the unsteady vortex structure arising when a single DBD plasma actuator is activated in quiescent air.

By controlling the duty cycle it results easy to control the intensity of actuation when low or moderate forcing is required. This becomes of interest when air flows at low velocity and an excessive forcing may be counterproductive.

It is also a crucial parameter as its value is directly related to the power consumed by the plasma actuator. For example, in our case an actuation with a duty-cycle of 100% consumes about 20 W while the electrical consumption with a duty-cycle of $\eta$% results in ($\eta$ x 20 W)/100.

The starting vortex dynamics (core trajectory and velocity) was reproduced quite well with the numerical simulation that mimics the actuation using a slip velocity distribution as a boundary condition. We also have shown that the observed behaviour of the vortex core dynamics, with respect to the duty cycle, can be satisfactorily explained using the same scaling laws that are used to analyze the junction vortex.

The experimental and numerical results are in good agreement showing the potential of this pseudo-empirical model approach to characterize the plasma actuation.

## References

[1] Boeuf J P and Pitchford L C 2005 Electrohydrodynamic force and aerodynamic flow acceleration in surface dielectric barrier discharge *J. Appl. Phys.* **97** 103307
[2] Font G I and Morgan W L 2005 Plasma discharges in atmospheric pressure oxygen for boundary layer separation control *AIAA Paper* 2005-4632
[3] Moreau E 2006 Airflow control by non-thermal plasma actuators *J. Phys.* D: Appl. Phys. **39** 1
[4] Soldati A and Banerjee S 1998 Turbulence modification by large-scale organized electrohydrodynamic flows *Phys. Fluids* **10** 1742-50
[5] Corke T C and Post M L 2005 Overview of plasma flow control: concepts, optimization and applications *AIAA Paper* 2005-0563
[6] Visbal M R, Gaitonde D V and Roy S 2006 Control of transitional and turbulent flows using plasma-based actuators *AIAA Paper* 2006-3230
[7] Rumsey C L et al. 2008 *CFL3D Version 6 web page* NASA Langley Research Center (`http://cfl3d.larc.nasa.gov`)
[8] Likhanskii A V, Schneider M N, Macheret S O and Miles R B 2006 Modeling of interaction between weakly ionized near-surface plasmas and gas flow *AIAA Paper* 2006-1204
[9] Opaits D F, Neretti G, Likhanskii A V, Zaidi S, Shneider M N and Miles R B 2007 Experimental Investigation of DBD plasma actuators driven by repetitive high voltage nanosecond pulses with DC or low-frequency sinusoidal bias *AIAA Paper* 2007-4532
[10] Ghosal S 2006 Electrokinetic Flow and Dispersion in Capillary Electrophoresis *Annu. Rev. Fluid Mech.* **38** 309–38
[11] Gronskis A, Sosa R and Artana G 2009 Modelling EHD Actuation with a Slip Velocity *Joint ESA/IEEE-IAS/IEJ/SFE/IEA Conf.* Boston, MA
[12] González L M, Artana G, Gronskis A and D'Adamo J 2009 A computational moving surface analogy of an electrodynamic control mechanism in bluff bodies *4th Symposium on Global flow instability and control* Crete, Greece
[13] Peers E, Ma Z and Huang X 2010 A numerical model of plasma effects in flow control *Phys. Lett.* A **374** 1501–4

[14] Enloe C L, McLaughlin T E, Gregory J W, Medina R A and Miller W S 2008 Surface potential and electric field structure in the aerodynamic plasma actuator *AIAA Paper* 2008-1103
[15] Settles G S 2001 *Schlieren and Shadowgraph Techniques: Visualizing Phenomena in Transparent Media* (Berlin: Springer-Verlag)
[16] Rodríguez Gallego A and González Gutiérrez L M 2003 *ADFC Navier-Stokes solver* (`http://adfc.sourceforge.net`)
[17] Allen J J and Naitoh T 2007 Scaling and instability of a junction vortex *J. Fluid Mech.* **574** 1–23